Research Article
Experimental and Translational Hepatology

JOURNAL
OF HEPATOLOGY

A single-cell atlas of the woodchuck liver reveals cellular programs conserved in human HBV infection

Authors

Zoe A. Clarke, Jawairia Atif, Xinle Wang, …, Ian D. McGilvray, Gary D. Bader, Sonya A. MacParland

Correspondence

s.macparland@utoronto.ca (S.A. MacParland).

Graphical abstract

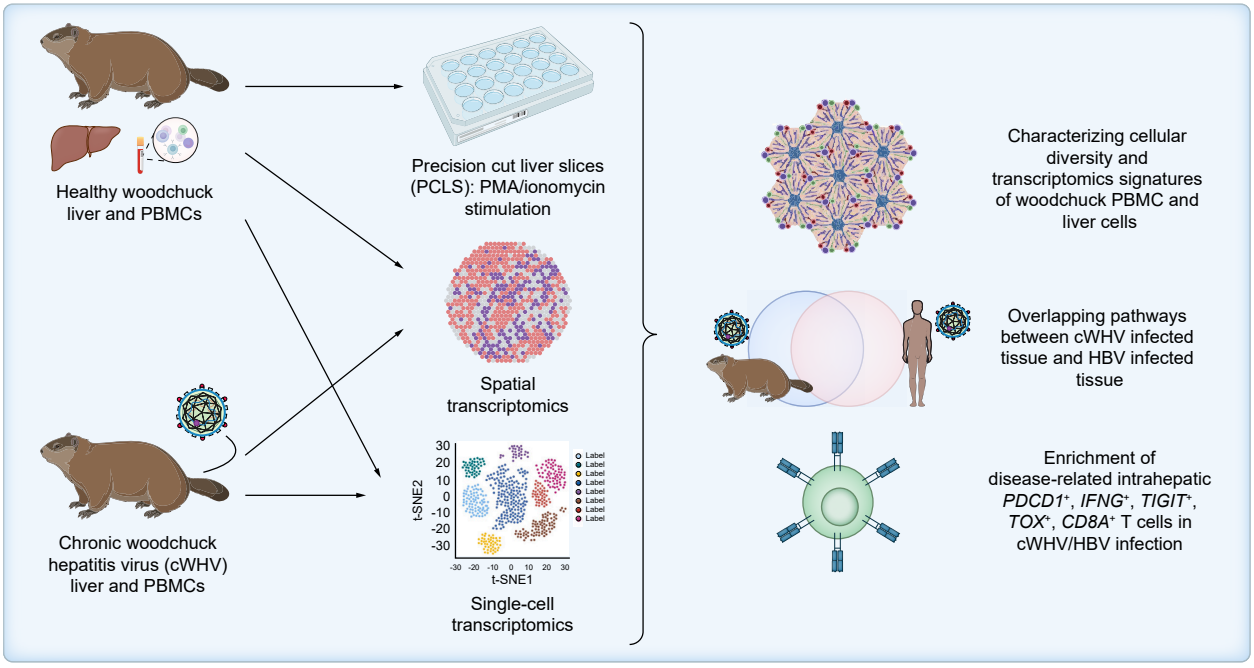

Highlights

- Woodchuck liver and blood cells share key characteristics with human cells.
- Analogous cells in liver and blood have unique signatures indicating their origin.
- Exhausted T cells are enriched in the diseased woodchuck liver.
- Woodchucks and humans share chronic hepatic inflammation gene signatures.

Impact and implications

Limited treatment options for liver disease, often culminating in the need for liver transplantation, underscore the requirement for human-relevant animal models to speed up the development of new therapeutic interventions. Woodchucks infected with woodchuck hepatitis virus develop chronic hepatitis and liver cancer, mirroring human HBV infection. However, the cellular composition and active biological processes within the woodchuck liver have remained poorly understood, limiting the model's utility for therapeutic discovery. In this study, we characterize the healthy and chronically infected woodchuck liver at single-cell resolution and compare it with human HBV infection, thereby reinforcing the value of the WHV-infected woodchuck as a model for human HBV disease.

https://doi.org/10.1016/j.jhep.2025.12.030
 J. Hepatol. 2026, 84, 962–975

Research Article
Experimental and Translational Hepatology

JOURNAL
OF HEPATOLOGY

A single-cell atlas of the woodchuck liver reveals cellular programs conserved in human HBV infection

Zoe A. Clarke[1,2,†], **Jawairia Atif**[3,4,†], **Xinle Wang**[3,†], Lewis Y. Liu[3,4], Lawrence Wood[3,4], Damra Camat[3,4], Yijia Liu[6], Ariya Shiwram[3], Sharon J. Hyduk[4], Sai Chung[3,4], Xue-Zhong Ma[4], Justin Manuel[4], Si Lok[5], Timothy N.H. Lau[5], Cornelia Thoeni[6], Tomasz I. Michalak[7], Ian D. McGilvray[4,‡], Gary D. Bader[1,2,8,‡], Sonya A. MacParland[3,4,6,‡,*]

Journal of Hepatology **2026**. vol. 84 | 962–975

Background & Aims: The eastern woodchuck (*Marmota monax*), which can be naturally infected with woodchuck hepatitis virus (WHV), has served as a model for studying aspects of human HBV infection, including the establishment of chronic infection and progression from chronic hepatitis to liver cancer. However, the cellular landscape of the woodchuck liver and its parallels to HBV infection remain uncharacterized.

Methods: We generated a single-cell and spatial transcriptomic atlas of the woodchuck liver in health and chronic WHV infection, characterizing cell types and infection-associated processes in hepatic tissue (healthy: 52,024 cells; infected: 40,810 cells; n = 8 per group) and peripheral blood mononuclear cells (healthy: 25,314 cells, n = 7; infected: 19,518 cells, n = 8). We further examined shared WHV–HBV disease pathways transcriptionally and assessed woodchuck liver immune responses functionally using PCLS (precision-cut liver slice) stimulation.

Results: Using this atlas, we found that hepatic cellular and immune diversity in the woodchuck liver is comparable to that of human livers. Immune cells in PMA/ionomycin-stimulated PCLS exhibited a robust type I inflammatory response, as expected, supporting the accuracy of our cell-type annotations. Our atlas further revealed transcriptional and cellular similarities between WHV- and HBV-infected livers, including periportal dendritic cell activation and a restructuring of the T-cell compartment from memory toward exhaustion during WHV infection, a hallmark of chronic human HBV.

Conclusions: We present a multi-omic atlas of healthy, diseased, and *ex vivo*-stimulated woodchuck liver. This work identified shared WHV–HBV pathological processes, reinforces the value of this preclinical model, and provides a resource to advance HBV pathogenesis studies and therapeutic development.

Introduction

The mammalian liver is a vital organ with essential metabolic and detoxification functions.[1–3] It has a profound regenerative capacity that can be compromised in end-stage disease, necessitating transplantation.[4] HBV is a hepatotrophic virus that can persist chronically in the infected host and can lead to hepatocellular carcinoma (HCC), the most common primary form of liver cancer.[5]

Investigations into the pathogenesis of HBV have been constrained by limited access to physiologically relevant animal models, restricted human tissue availability, and the inherent fragility of hepatic cell populations.[1,6] While single-cell RNA sequencing (scRNA-seq) and spatial transcriptomics have advanced our understanding of hepatic cellular complexity, the lack of a well-characterized HBV animal model precludes functional studies of disease progression and therapeutic intervention.[1,7]

The eastern North American woodchuck, *Marmota monax*, can be naturally infected with woodchuck hepatitis virus (WHV) and serves as a critical immunocompetent preclinical model for HBV-induced liver disease.[8,9] WHV mirrors human HBV in genome organization, and the infection causes an immune response, and disease progression from hepatitis to HCC reflective of human disease.[8,9] This model has helped reveal key insights into chronic HBV persistence, but its full potential is limited by scarce woodchuck-specific cell biology resources for tracking cellular ecosystems during WHV infection.[10–12]

Here, we mapped the healthy and WHV-infected woodchuck liver and matched peripheral blood mononuclear cells (PBMCs) using scRNA-seq, spatial transcriptomics, and *in vitro* tissue stimulation studies (Fig. 1). We applied this map to

* Corresponding author. Address: Department of Immunology, University of Toronto, Toronto, Ontario Canada.
E-mail address: s.macparland@utoronto.ca (S.A. MacParland).
† Equal contribution co-first authors.
‡ Equal contribution senior authors
https://doi.org/10.1016/j.jhep.2025.12.030

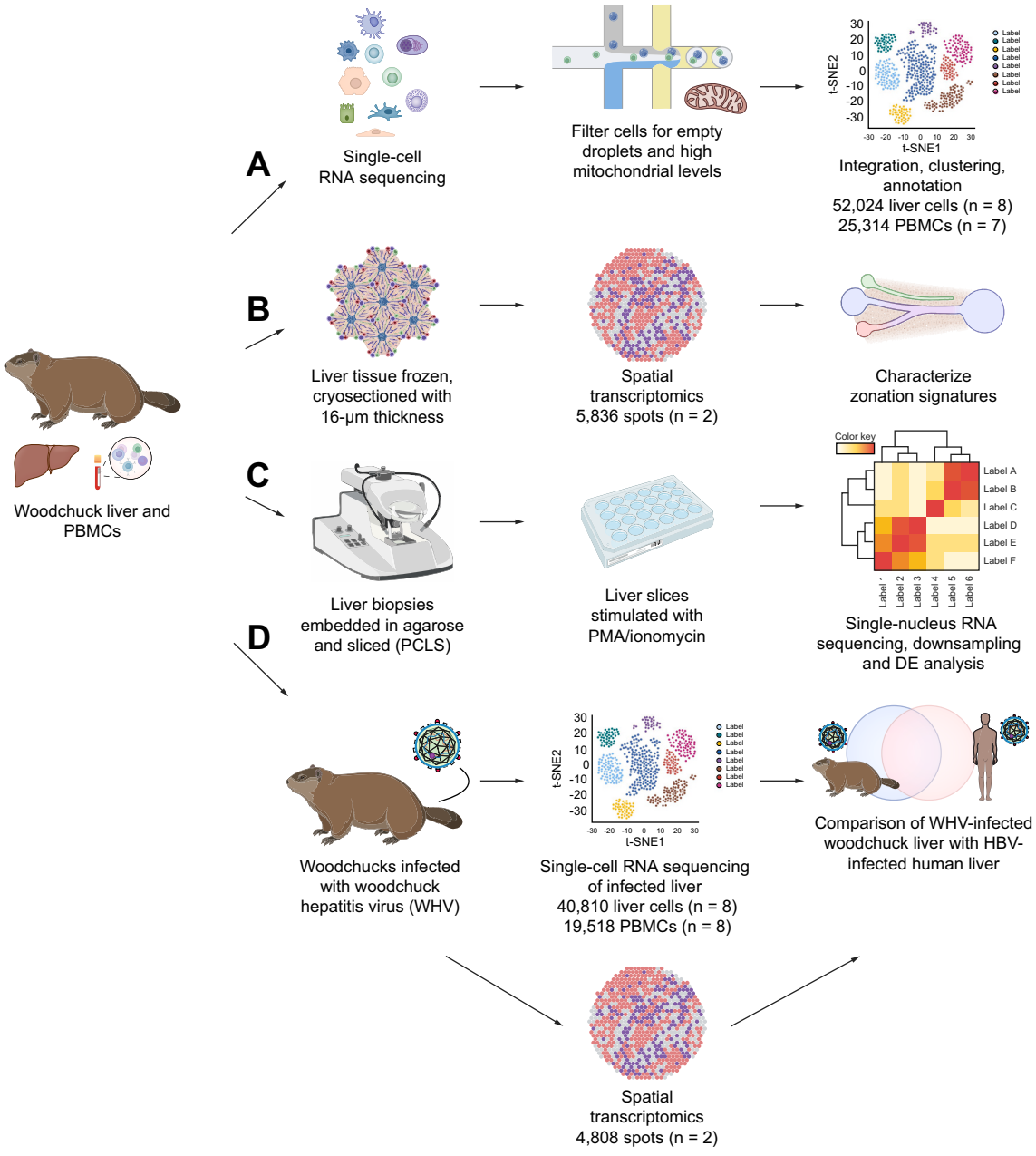

Fig. 1. Generation of the healthy woodchuck liver atlas and its application to cWHV/cHBV. (A) Intrahepatic cells (eight healthy livers) and PBMCs (seven matched samples) underwent scRNA-seq, quality filtering, and clustering/annotation. (B) Spatial transcriptomics data from one healthy liver (two slices) were processed with 10X Genomics pipeline and zonation signatures characterized. (C) PCLS were stimulated with PMA/ionomycin, followed by single-nucleus RNA sequencing, downsampling, and comparison to unstimulated controls. (D) scRNA-seq (eight liver samples, eight PBMC samples) and spatial transcriptomics (one liver, two slices) were performed on cWHV cells. The scRNA-seq samples were merged with healthy cells and compared to HBV-infected liver data.[13] cHBV, chronic hepatitis B virus; cWHV, chronic woodchuck hepatitis virus; PBMCs, peripheral blood mononuclear cells; PCLS, precision-cut liver slices; PMA, phorbol 12-myristate 13-acetate; scRNA-seq, single-cell RNA sequencing. (This figure appears in color on the web.)

examine WHV-induced disease pathways and identified overlapping T-cell exhaustion and dendritic cell differentiation and activation pathways in chronic WHV (cWHV)-infected woodchuck livers and human chronic HBV (cHBV) infection, including *TIGIT*, *TOX*, *PDCD1*, and *IFNG*. This analysis provides a foundation for cell-specific studies of HBV liver pathogenesis and oncogenesis, and for preclinical evaluation of new therapies for cHBV and HCC.

Materials and methods

Details regarding tissue and transcriptomic data processing and data analysis can be found in the supplementary methods.

Tissue preparation

All animal procedures included in this study were approved by institutional ethics boards (supplementary methods).

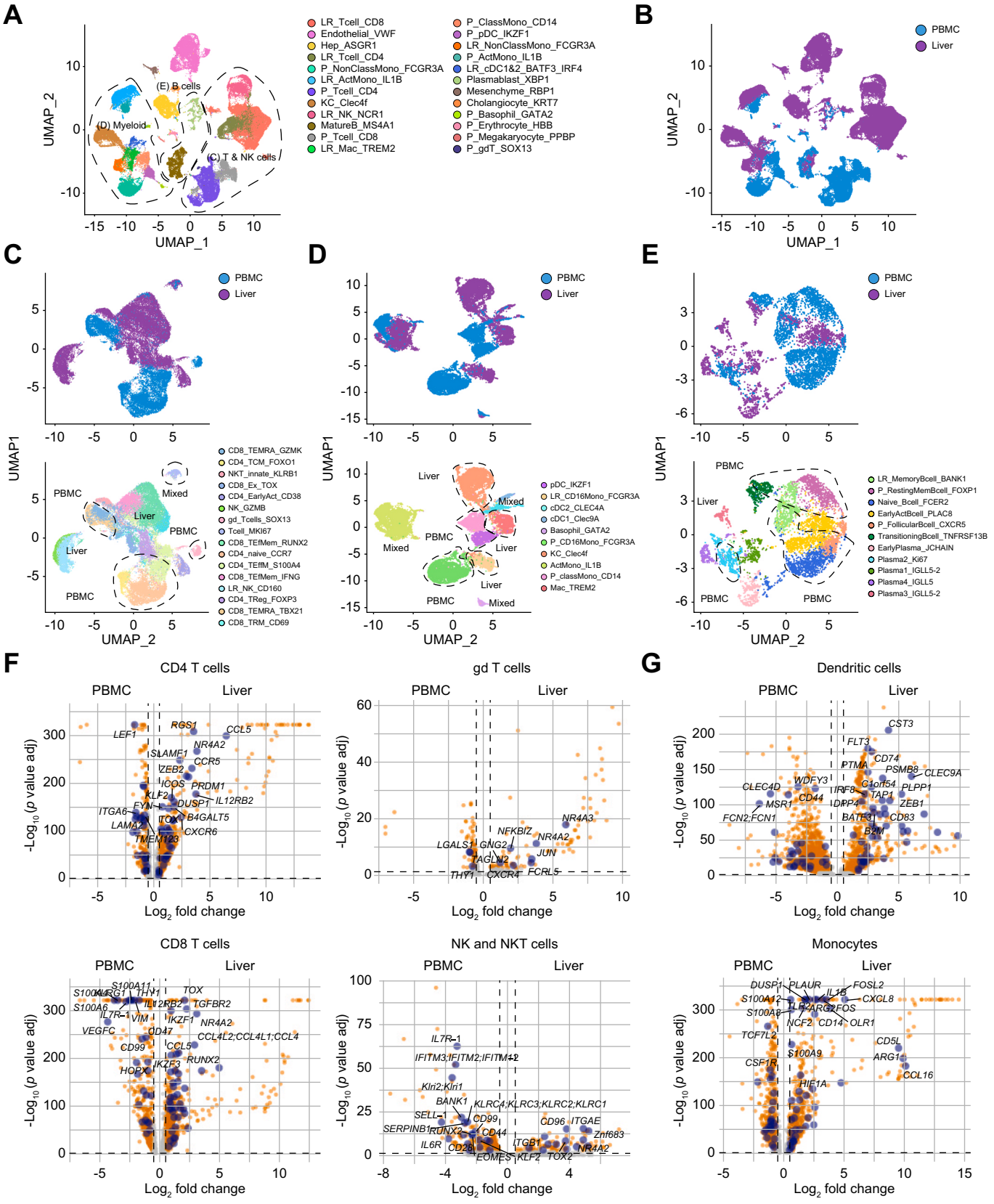

Fig. 2. Woodchuck liver and PBMCs show distinct populations of circulating and tissue-resident immune cells. (A) A total UMAP of 77,338 cells from woodchuck liver biopsies (n = 6), liver homogenate from perfused caudate lobes (n = 2), and PBMCs (n = 7) with annotations assigned and coarse cell types used for subclustering circled. (B) Total UMAP colored by tissue type. (C-E) Zoom-in subclustering of NK cells and T cells (C), Myeloid cells (D) and B cells (E) (clusters from total map included in each zoom-in are indicated in Fig. 2A), upper panels show UMAPs colored by tissue type, lower panels show annotated clusters for each zoom

Woodchucks (see clinical and virological characteristics, Table S1) were infected with WHV under established protocols and liver tissue was dissociated into single-cell suspensions as previously described.[1,14] PBMCs were isolated using standard percoll-based density gradient centrifugation.

Precision-cut woodchuck liver slice stimulations

Precision-cut liver slices (PCLS) were generated from woodchuck W3391 (healthy) and stimulated for *ex vivo* studies as previously described, and single-nucleus RNA-seq (snRNA-seq) was performed on the stimulated slices.

RNA-sequencing and data processing

We developed a new, annotated high-quality woodchuck genome annotation to enable gene identification and quantification from RNA-sequencing data (Fig. S1, details in the supplementary methods). 3′ Visium spatial transcriptomics (10x Genomics; see Table S2 for sample QC) was performed on OCT-embedded 16-μm slices from healthy (L212) and diseased (L215) woodchuck liver tissue, and scRNA-seq and snRNA-seq data (10x Genomics Chromium Single Cell 3′ v2 chemistry) were aligned to the woodchuck genome using 10x Genomics Space Ranger v1.2.2 and Cell Ranger v5.0.0, respectively. Sequencing data were processed, integrated, and annotated using the seurat v5 analysis[15] pipeline, and DropletQC[16] was used to remove empty droplets in filtered Cell Ranger results (Figs. S2 and S3). Shared immune dysfunction between cWHV and cHBV infections was examined *via* pathway analysis using publicly available human HBV data (GSE182159).[13]

DNA extraction and quantitative WHV PCR

DNA was isolated from 100 μl plasma or 10 mg of snap-frozen tissue and was amplified by quantitative PCR using WHV and woodchuck b-actin specific primers. Cycling conditions were as follows: 95 °C for 1 min followed by 45 amplification cycles (95 °C for 15 s, 60 °C for 30 s) and a melt curve. Primers against the WHV preS region were used at a final concentration of 250 nM (forward: ATGCACCCATTCTCTCGAC; reverse: CTGAGCAGCTTGGTTAGAGT). Standard curves were generated using serial dilutions of WHV plasmid DNA from 108 to 1 copies/reaction. The WHV viral copies are reported as copies per ml of plasma or ng of total DNA. Full details can be found in the supplementary methods.

Results

An atlas of healthy woodchuck liver cells and PBMCs demonstrates compartment-specific immune subtypes and transcriptional profiles

After filtering, scRNA-seq of six liver biopsies and two perfused lobes yielded 52,024 liver cells and 25,314 PBMCs, which were broadly grouped into 24 cell types (Fig. 2A–E and S4). Our combined atlas of woodchuck liver and PBMCs was annotated with automated methods based on human datasets,[1,2,17,18] (Fig. S5) and manual curation focused on lineage-associated genes from human liver single-cell studies (Table S3, Figs. S6–S10). Our approach to include biopsies and perfused caudates captured both liver parenchymal (hepatocytes and cholangiocytes) and non-parenchymal cell populations (endothelial and mesenchymal cells, Figs. S6 and S7), and immune cell populations (myeloid cells, T cells, NK cells, and mature and antibody-secreting B cells, Figs. S8–S10) based on transcriptomic similarity to their human counterparts (Fig. S5).

With these annotations applied (Fig. 2A), we first employed the atlas to examine infiltrating immune cells in woodchuck liver homogenates *vs*. those found in PBMCs to allow for a more accurate description of tissue residency genes. Cell types captured from the woodchuck liver and PBMCs largely separated into unique populations, except for basophils, plasmablasts, and mature B cells (Fig. 2B–E and S4A-F). Our analysis yielded numerous immune tissue residency markers in woodchuck liver. Just as in human datasets,[1,2] tissue-resident immune cells had distinct gene expression profiles from circulating populations of the same cell type (Fig. 2FG, and S11, Table S3). Liver-resident T-cell and NK cell populations (Fig. 2F) had clear markers of tissue residency (*e.g. CXCR6, ITGAE, ITGB1, CCL5*)[19,20] and differentiation (*e.g. RUNX2, KLF2, TOX, ZBE2, NR4A2*).[19,20] In contrast, PBMC-enriched T-cell and NK cell populations expressed circulating (*e.g. CCR7, SELL*)[21] and resting (*e.g. LEF1, SATB1*)[13] phenotypes. Further differences in gene expression by compartment were noted in the NK and NKT cell subclusters (Fig. S11), with those found in the liver predominantly sharing markers of lymphocyte terminal differentiation (*e.g. GZMK, NKG7*), while expressing liver-resident T and NK cell genes (*e.g. FCER1G, GZMH/B, CD160, Znf683*). Meanwhile NK and NKT cell subclusters from PBMCs differentially expressed *IL7R, BANK1, SELL-1,* suggesting the adoption of a residency and differentiated phenotype in the liver.

Myeloid populations also displayed compartmentalization, with dendritic cells, basophils *(GATA4)*, and activated monocytes *(IL1B)* distributed across both sites, while macrophages *(C1QC)* and Kupffer cells *(MARCO, C1QC)* were liver-enriched (Fig. 2D). Furthermore, dendritic cells in PBMCs (Fig. 2G) expressed genes related to inflammation (*e.g. FCN1, FCN2, MSR1*),[22] while those in the liver expressed genes associated with antigen-presentation to $CD8^+$ T cells and differentiation (*e.g. CD74, TAP1, CLEC9A, BATF3, IRF8, FLT3*).[23] Taken together, this atlas provides a platform for examining the PBMC to liver immune cell differentiation, activation and infiltration trajectories and the transcriptomic signatures of woodchuck intrahepatic cell populations.

Spatially resolved woodchuck liver transcriptomics reveal hepatocyte metabolic programs

Hepatocytes exhibit zonated gene expression patterns, with periportal cells specializing in high-energy processes like

in. (F-G) Volcano plots showing the expression of tissue residency (right) and PBMC-associated (left) genes in subclustered immune cells from woodchuck liver and PBMCs, with key human genes highlighted. The four T/NK cell volcano plots correspond to clusters in panel C and are annotated with CD4, CD8, γδ, and NK, respectively. The two myeloid volcano plots correspond to clusters in panel D and are annotated with DC and Mono, respectively. DC, dendritic cell; PBMCs, peripheral blood mononuclear cells; UMAP, uniform manifold approximation and projection. *p*-values were calculated using the Wilcoxon rank-sum test. (This figure appears in color on the web.)

cholesterol biosynthesis and oxidative metabolism, while pericentral cells focus on glycolysis and xenobiotic metabolism.[3] Unbiased spatial transcriptomics with 55 μm resolution (10X Genomics 3' Visium) was applied to ascribe a geographical location to the annotated intrahepatic cells in our atlas. This approach provided spatial context to periportal and pericentral hepatocytes revealing their distinct transcriptional profiles (lobule zones annotated by a pathologist, Fig. 3A–E, Tables S4–S6). Pericentral hepatocytes differentially expressed human pericentral markers (*CYP2E1*, *FETUB*, *CYP1A2*) alongside *GLUD1/GLUD2* (non-zonated in humans) and *HMGCS1* (periportal in humans), indicating partially conserved but distinct zonation patterns between species.[1,17] Using pathway analyses, we found that enriched pathways in the pericentral zones include those of xenobiotic metabolism, blood coagulation, bile transport, and demethylase activity (Fig. 3F), which is consistent with what has been recorded in the literature.[3,24]

Periportal hepatocytes in the woodchuck shared both human periportal markers *HAMP, APOC2,* and mouse orthologs *Saa1/Saa2* (Fig. 3D,E, Tables S4 and S5). Pathway enrichment analysis of periportal zones from the spatial transcriptomics data revealed triglyceride regulation, alcohol binding, hormone binding, and electron respiratory chain pathway activity (Fig. 3F). Combining this evidence demonstrates strong correlations with human and mouse biology in liver zonation.

As described previously,[1,17,24] hepatocyte markers were a source of ambient RNA contamination in scRNA-seq data, indicating that they may have been damaged or otherwise influenced by the experimental protocol, limiting the ability to resolve hepatocyte transcriptional profiles in the scRNA-seq data (Fig. S12).

As expected,[1,17,24] in the Visium spatial data from 55 μm-diameter spots, hepatocyte signatures were dominant over those of other smaller cell types, making the localization of non-hepatocytes difficult to resolve. For example, *VWF* and *ACKR1,* markers for periportal and pericentral endothelial cells, respectively (Fig. S6), have correlation coefficients of -0.01 and 0.01 with their respective zones when analysing the spatial transcriptomics data (Table S6). Other marker genes have similarly weak coefficients, suggesting that co-occurring signals were not sufficiently strong to draw any conclusions (Table S6) and that a higher resolution spatial approach or a probe-based approach targeting non-hepatocyte genes would be required.

Examination of woodchuck intrahepatic cell function using PCLS

To validate our annotations and characterize woodchuck cell-specific responses, we stimulated woodchuck PCLS *in vitro* with phorbol 12-myristate 13-acetate (PMA) and ionomycin before snRNA-seq analysis (Figs 1C and 4A). PMA triggers receptor ligation-independent NF-kB pathway activation, while ionomycin increases intracellular calcium, a critical mediator of immune activation.[25] We identified cell types based on their gene expression profiles (Fig. 4B, Table S7), and compared PMA-stimulated cell populations to their unstimulated counterparts on a per-lineage basis (Fig. 4C–G, Table S8). Generally, type I inflammation gene signatures were strongly expressed in stimulated T and myeloid cells, with mild inflammation signatures occurring in other cell types (Fig. 4D–G, Table S8). Firstly, PMA-stimulated T cells expressed known activation markers (*NFKB1, CCL3, CCL4, CCL5, TNF,* and *IL2RA)* and showed TGFβ signalling and IFNγ activation (Fig. 4D–E,G, Table S8). This response mirrored previously reported human PBMC T-cell responses to PMA/ionomycin, which showed corresponding upregulation of *IL2, IFNG, TNF-α*, and *CCL5* (RANTES).[25] Collectively, this suggests a bias towards TH1 over TH2 or TH17 responses. Stimulated myeloid populations similarly upregulated *NFKB1, TNF, IFNG, IL2RA, CCL4,* and *CCL3*, along with *IL7* (Fig. 4F,G), with pathways enriched for interferon response, inflammation, and chemokine migration (Fig. S13). Myeloid-specific activation markers *SLAMF1*, *CD274*, *GBP2*, *CXCL8* and *BATF2* were also induced (Fig. S14), validating the presence of anticipated inflammatory signatures.

Beyond immune cells, hepatocytes, cholangiocytes, endothelial cells, and mesenchymal cells similarly displayed pro-inflammatory *NFKB1* pathway activation seen through upregulation of key cytokines: (*CXCL10*, *CCL4* and *CXCL8)*, and inflammatory effector proteins (*TIFA* and *IDO1)* (Fig. 4D,G and S14, Table S8). Further, stimulated hepatocytes expressed *FAS* while cholangiocytes upregulated caspase transcripts (*CASP4*, *CASP6)* (Table S8), suggesting an activation of cell-death programs in parenchymal cells. Endothelial cells also increased the expression of cell adhesion and leukocyte trafficking markers (*e.g*. *CD44*, *ITGAM*, *SYN3*, and *VCAM1*), Type I inflammation genes *(STAT3, IFNG)* and pro-survival genes (*e.g. BATF3*, *IRGM*, *TCF3*), underscoring the role of these cells in activating the immune response and promoting immune infiltration (Fig. 4D,G, Table S8). Furthermore, cholangiocytes and endothelial cells showed increased expression of *CSF1* (Table S8), a monocyte to macrophage differentiation growth factor. Antibody-secreting B cells, myeloid cells and hepatocytes also showed increased expression of lymphocyte growth factor gene *IL7* (Fig. 4D,G, Table S8). Altogether this suggests the upregulation of a macrophage-promoting environment and the development of a T-cell supportive niche in inflammatory liver tissue. Collectively, these findings demonstrate that woodchuck hepatic cells exhibit coordinated inflammation-associated gene activation following PMA/ionomycin stimulation.

Periportal zone damage and cytotoxic T-cell exhaustion in cWHV infection

To expand on the value of the woodchuck as a pre-clinical model of chronic viral liver infection, we applied our scRNA-seq workflow to cWHV-infected woodchuck livers (Figs. 1D, 5A,B, and S15-S21). Using the marker genes identified through the above analysis, 23 populations of parenchymal, stromal, and immune cells were annotated (Figs. S15A-F and S20-S25; diseased animal characteristics, Table S1; cell-type-specific differential gene expression analysis, Table S9; diseased *vs.* healthy differential gene expression analysis for each cell type, Table S10; histology, Fig. S16–S19). Cells from infected livers strongly and consistently expressed WHV viral transcripts while healthy samples did not (Fig. 5C–E).

Analysis of the infected spatial transcriptomic liver slices from woodchuck L215 revealed strong pericentral zonation, but very little periportal zonation, suggesting a reduction of periportal gene expression in response to infection (Fig. 5F,G). Specific cell type signatures were differentially present

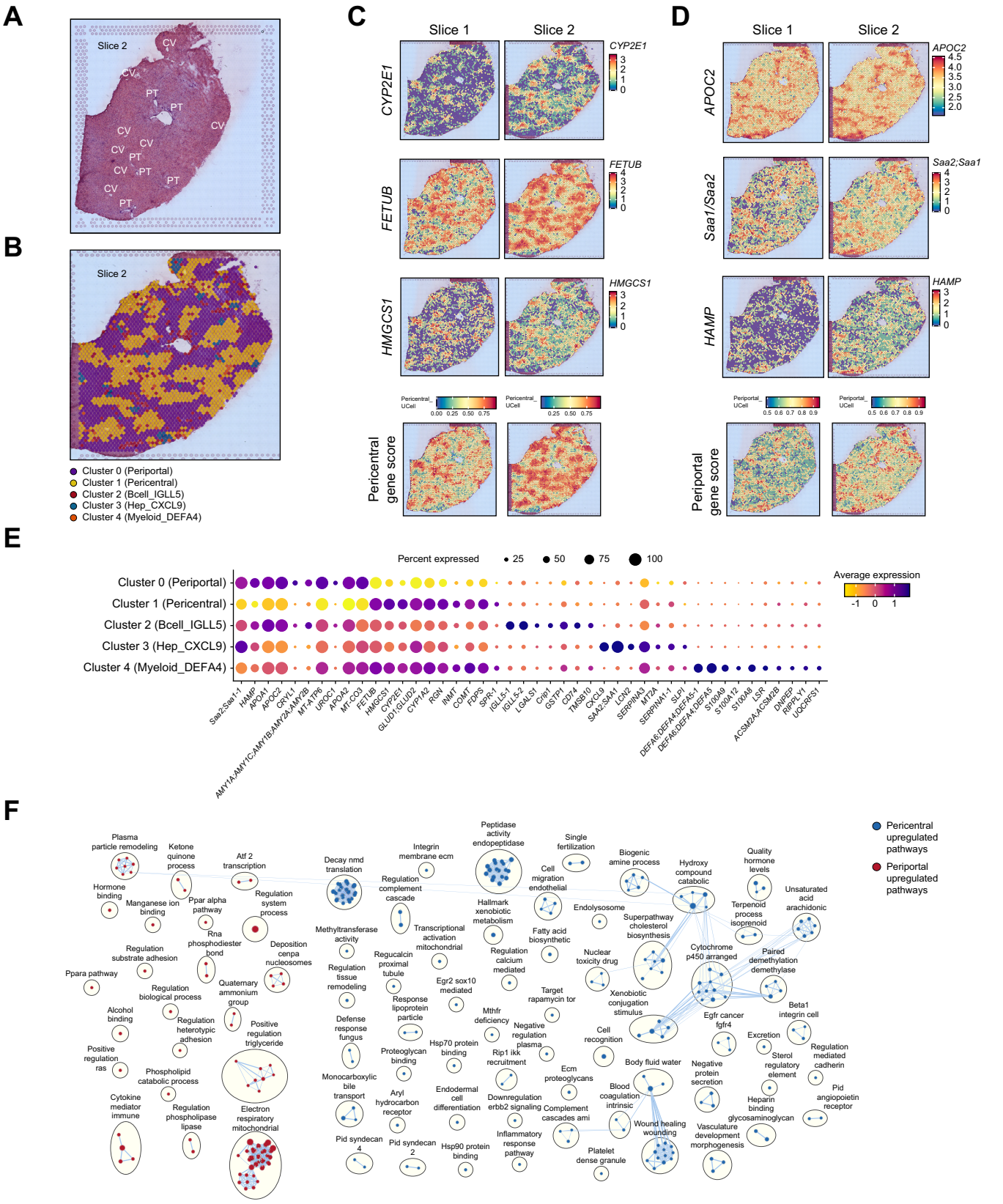

Fig. 3. Spatial transcriptomics data describes zonation patterns in the woodchuck liver. Spatial transcriptomics of two healthy woodchuck liver slices. (A) H&E-stained liver with pericentral/periportal zonation. (B) Spatial clusters projected onto the liver slice. (C) Key pericentral genes (*CYP2E1, FETUB, HMGCS1*) and gene score and (D) periportal genes (*APOC2, Saa1/Saa2, HAMP*) and gene score mapped onto slices. (E) Spatial clusters and key spatial-associated genes projected as dotplots. (F) Pathways upregulated for periportal (red) and pericentral (blue) hepatocytes. **AMY2B* truncated from *AMY1A;AMY1C;AMY1B;AMY2A;AMY2B*. (This figure appears in color on the web.)

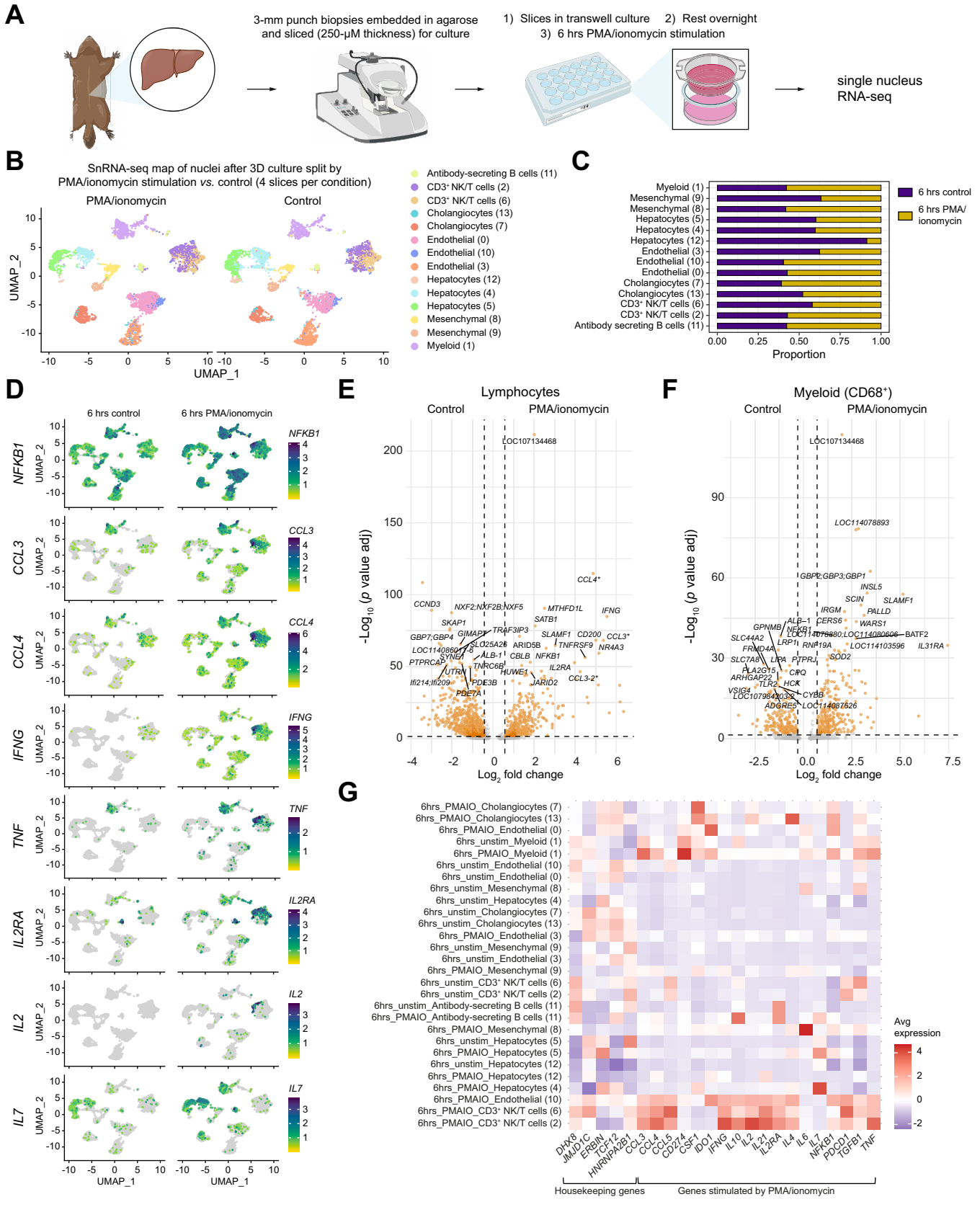

Fig. 4. PMA/ionomycin stimulates immune cell populations in the woodchuck liver. (A) Healthy woodchuck precision cut liver slices were stimulated with PMA/ionomycin and snRNA sequencing was performed. (B) A UMAP of 9,208 stimulated and unstimulated woodchuck liver cells split by treatment and labelled by cell type. (C) A barplot of sample IDs as distributed across clusters labelled in (B) where UMAPs are split by treatment (PMA/ionomycin and control, respectively). (D) UMAPs of stimulated woodchuck liver cells split by sample ID with heatmaps of key inflammatory genes projected onto the maps. (E) and (F) are volcano plots of the

between healthy and diseased spatial transcriptomics data (Fig. 5H) and were enriched in specific zones (Fig. 5I and S22).

We identified a cluster of T cells (CD8_Ex_TOX) with upregulation of key effector- (*IFNG, KLRD1, CCL3*), activation- (*FUT8*), and exhaustion-associated markers (*TOX, NR4A2*) in cWHV that were enriched in disease (Fig. 6A–E and S17). Additionally, NK/T cells in healthy woodchuck liver and PBMC samples had a higher cytotoxic score while maintaining a lower exhaustion signature than cWHV NK/T cells (Fig. 6D, Table S11 for gene sets). These data indicate that $CD8^+$ T cells may be exhausted in cWHV-infected livers, leading to impaired viral clearance in chronic infection, similar to findings from recent scRNA-seq studies of cHBV-infected human livers.[13]

In addition, dendritic cells also expressed distinct genes in infected *vs*. healthy cells, largely involved in differentiation or antigen presentation (*e.g. CADM1, WDFY4, IRF8, LRBA*) (Fig. 6F). Myeloid cell populations were generally more abundant in the diseased spatial transcriptomics data compared with healthy tissue, with stronger signature scores for classical monocytes, Kupffer cells, activated monocytes, and dendritic cells, among others (Fig. 6G).

Furthermore, similar to cHBV infection,[26] histological evaluation of cWHV-infected tissue identified immune infiltration, and mild hepatocytic necrosis at the periportal region while the central veins remain undamaged (Figs. S23–S26). This supports the reduced periportal zonation seen in the spatial transcriptomics data (Fig. 5F). Altogether these results suggest a reduction in healthy periportal hepatocytes and increased exhausted T cells and immune filtration in the liver during cWHV infection.

Cell-level characterization of cWHV infection as a preclinical model of cHBV infection

To directly compare cWHV infection with cHBV, we analysed a publicly available dataset of immune-active cHBV-infected scRNA-seq data of immune cells (GSE182159).[13] Shared markers of chronic activation were identified by correlating genes upregulated in both cWHV and cHBV relative to their respective healthy controls (Fig. 7A). The strongest correlations were observed in $CD8^+$ T cells, where shared markers included exhaustion-associated genes *TOX* and *NFATC1* as well as T-cell activation markers, *TNFRSF1B, NR4A2, ITGB1 and CD27*.[13] Several of these T-cell activation genes have also been shown in studies of liver-resident T cells in both MASH and cHBV infection.[27,28]

We then searched for shared enriched pathways in T cells and myeloid cells in both cWHV-infected woodchuck and HBV-infected human tissues (Fig. 7B,C). This analysis showed shared PD-1 activation, lymphocyte activation and pathways associated with myeloid activation such as “IFNG signalling” in chronic WHV carriers – reinforcing the parallels between cWHV and cHBV. This analysis indicates that cWHV-infected woodchuck livers exhibit disease-related pathway activation similar to that observed in human cHBV infection.

Previously, PD-1, a programmed cell death receptor that is expressed on activated effector T cells, has been shown to increase intrahepatically as a result of cWHV infection when analysed with quantitative PCR.[29] To further explore the shared PD-1 pathway and distinguish exhaustion from activation, we examined key activation and exhaustion genes and found that, in both cHBV and cWHV infection, T cells upregulated genes involved in exhaustion and inflammation (*TIGIT, TOX, TNFRSF9, CTLA4, IFNG, CXCR6*) (Fig. 7D and S27A-E). These findings suggest that similar programs are activated in both cWHV and HBV infections and highlights the potential and value of the woodchuck model for testing immunomodulatory interventions to drive antiviral immunity and promote a functional cure for HBV.

Discussion

A key challenge in using the WHV-infected woodchuck model to study HBV immunopathogenesis and target the intrahepatic cellular ecosystem has been the lack of molecular biology tools to characterize the cellular ecosystems within the woodchuck liver and circulating immune populations.[29–31] Here, we generated the first single-cell atlas of the woodchuck liver and PBMCs and used it to identify shared cell populations and gene pathways between WHV-induced disease in woodchucks and HBV infection in humans. Our atlas strengthens and reaffirms the translational potential of this unique, HBV-homologous model and will allow for the examination of key molecular parallels between WHV and human HBV pathogenesis to inform future therapeutic development.

Our cell-level examination of the parenchymal and non-parenchymal ecosystem in the healthy and diseased woodchuck liver delivers an unbiased snapshot of the major cell types, which compliments previous woodchuck studies and adds a new level of information regarding cell level interactions that may be targeted to promote antiviral responses. For example, previous bulk RNA-seq analyses have identified intrahepatic expression of markers associated with T-cell exhaustion and inhibition of antiviral cytokine signalling in livers of woodchucks with cWHV hepatitis.[30,32] Here, we characterize the transcriptome of exhausted-like T-cell populations derived from the liver of cWHV-infected woodchucks. These T cells, associated with viral persistence, express TOX, TIGIT, and CXCR6, and are present only in small numbers in the healthy woodchuck liver or PBMCs. Importantly, our data suggest that T-cell responses in cWHV and cHBV share similar dynamics, reinforcing the value of the woodchuck model for future studies aimed at modulating immunity to induce strong antiviral responses and achieve sterilizing HBV clearance. Indeed, restoring the function of exhausted T cells through reprogramming their metabolism is thought to be a promising therapeutic target for cancer immunotherapy.[33]

Previous studies that employed quantitative PCR to profile the immune infiltrates in biopsies from WHV-infected woodchucks have implicated intrahepatic regulatory T cells in

results of a differential expression test comparing slices stimulated by PMA/ionomycin to unstimulated cells. (E) Is a volcano plot of CD3+ NK/T cells, and (F) is a volcano plot of CD68+ myeloid cells. For both volcano plots, *p*-values were determined with the Wilcoxon rank-sum test. (G) Heatmaps showing the expression of housekeeping genes and genes stimulated by PMA/ionomycin. **CCL3* truncated from *CCL3L1;CCL3L3;CCL3;CCL18* and *CCL4* truncated from *CCL4L2;CCL4L1;CCL4*. PMA, phorbol 12-myristate 13-acetate; snRNA-seq, single-nucleus RNA sequencing; UMAP, uniform manifold approximation and projection. (This figure appears in color on the web.)

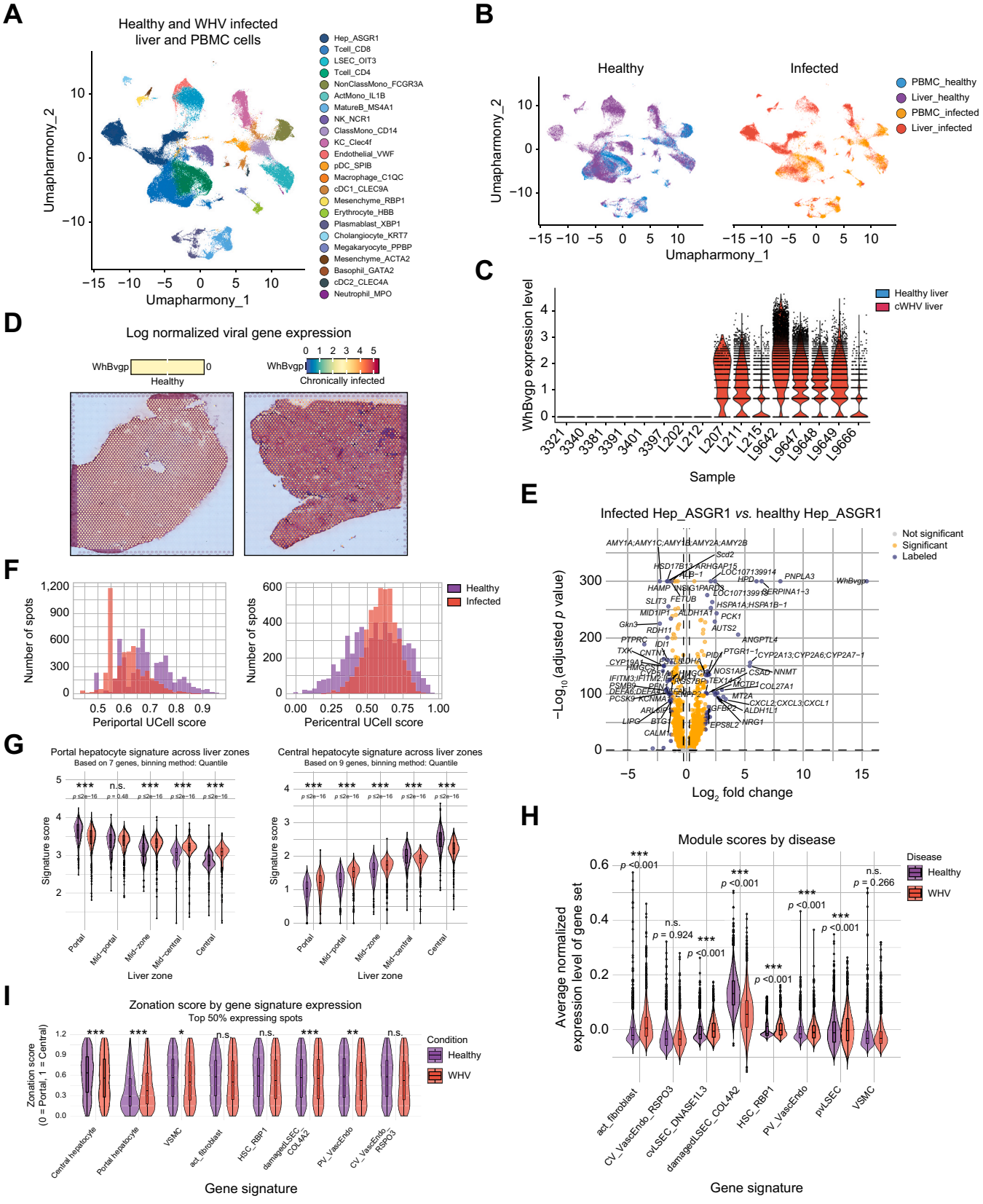

Fig. 5. A comparison of cWHV and healthy parenchymal and stromal cells. (A) UMAP of healthy and cWHV liver cells and PBMCs. (B) Cells split by disease state. (C) Normalized WHV expression across woodchucks. (D) The expression of WHV in spatial transcriptomics data. (E) Differentially expressed genes in infected (right) *vs.* healthy (left) hepatocytes. (F) The distribution of periportal and pericentral scores in healthy and infected spatial transcriptomics data and (G) across liver lobule spots. (H) Cell type scores in diseased and healthy spatial data and (I) the distribution of the zonation score within spots representing each cell type. Statistical significance in (E), (G), (H), and (I), was determined using the Wilcoxon rank-sum test with *** indicating p <0.001, ** indicating p <0.01, and * indicating p <0.05. (c)WHV, (chronic) woodchuck hepatitis virus; PBMCs, peripheral blood mononuclear cells; UMAP, uniform manifold approximation and projection. (This figure appears in color on the web.)

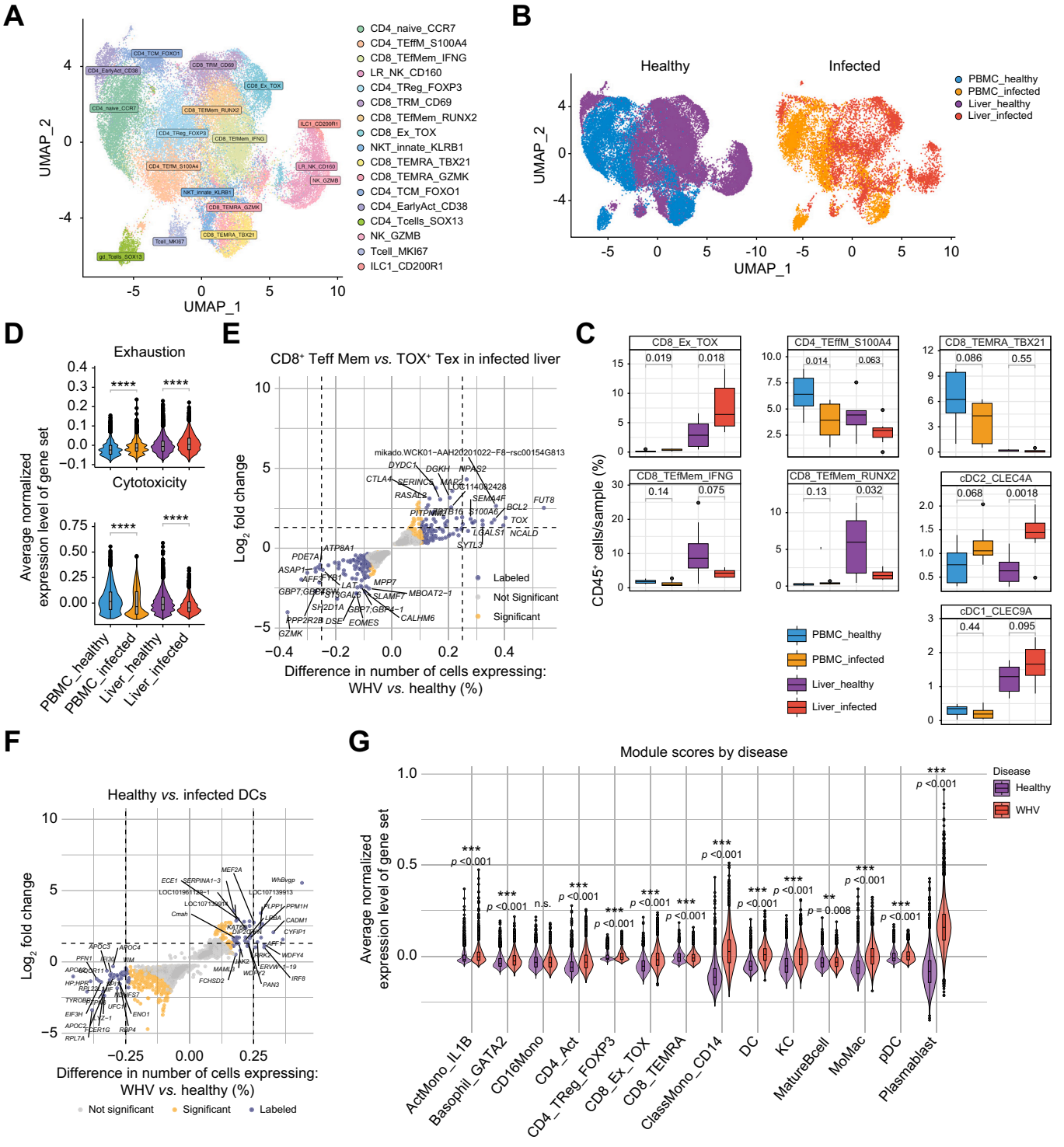

Fig. 6. The immune landscape of WHV-infected woodchuck blood and liver compartments. (A) A UMAP of healthy and diseased NK/T cells. (B) T cells from (A) split by disease state. (C) Proportion of immune cells within CD45$^+$ population. (D) A comparison of exhaustion and cytotoxicity scores. (E) A comparison of log-fold change and the proportion of cells that express a particular gene between CD8$^+$ Teff Mem (left) and Tox$^+$ Tex (right) and (F) infected (right) *vs*. (left) healthy DCs. (G) Cell type signatures across healthy and diseased cell subtypes in Visium data. Statistical significance comparing cell-type proportions in (C) was calculated with t-tests, and the significance of gene-set and gene expression differences in (D), (E), (F), and (G) was assessed with the Wilcoxon rank-sum test (*** indicates p <0.001, ** indicates p <0.01, and * indicates p <0.05). DC, dendritic cell; Teff Mem, effector memory T cell; Tex, exhausted T cell; UMAP, uniform manifold approximation and projection; WHV, woodchuck hepatitis virus. (This figure appears in color on the web.)

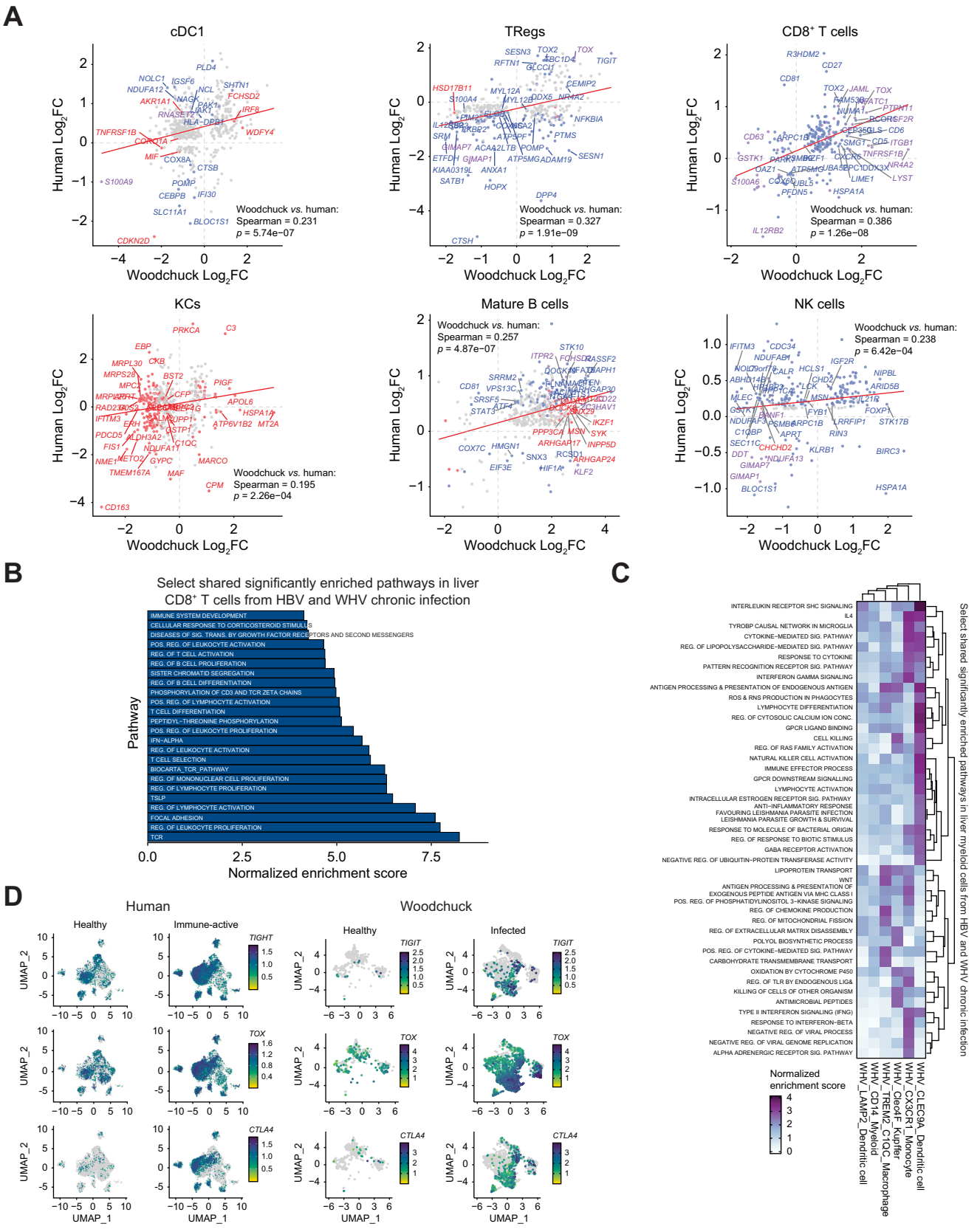

Fig. 7. Shared pathways of T-cell exhaustion and activation in cWHV- and cHBV-infected tissue. (A) The average log_2FC of each gene in the infected HBV and cWHV samples relative to their respective controls (red indicates significant in woodchuck, blue indicates significant in cHBV immune-active, purple indicates significant in both) across cell types. (B) Overlapping enriched pathways in gene-set enrichment analysis between T cells from cHBV (n = 5)[16] and cWHV (n = 8) livers. (C) Overlapping enriched pathways in gene-set enrichment analysis between infected myeloid populations. (D) UMAPs depicting the average normalized expression of exhaustion genes in both humans and woodchucks. cHBV, chronic hepatitis B virus; (c)WHV, (chronic) woodchuck hepatitis virus; FC, fold change; UMAP, uniform manifold approximation and projection. (This figure appears in color on the web.)

regulating, and specifically inhibiting, the response to HBV.[29,32] We found that intrahepatic regulatory T cells in the woodchuck liver are characterized by the expression of *FOXP3* and inhibitory genes *TOX* and *TIGIT*, in addition to upregulating the PD-1 pathway. Myeloid and dendritic cells have also been suggested to be involved in the immunopathogenesis of cWHV infection, noting an increase in their proportions weeks after infection.[29] However, myeloid cells in the infected liver have demonstrated toll-like receptor suppression, suggesting inhibition of innate immune function.[34]

In our study, in addition to the T-cell exhaustion and inhibitory signatures that were identified, our analysis simultaneously found pathways associated with the myeloid regulation of T cells. This further suggests that myeloid cells play an important role in guiding the T-cell response to viral infection. Taken together, our data shows shared myeloid activation and T-cell dysfunction in WHV and may provide a rationale for targeting T-cell and myeloid interactions as a potential pathway to modify or limit WHV-induced T-cell exhaustion and viral persistence.

We applied spatial transcriptomics profiling to probe hepatocyte zonation within the woodchuck liver, identifying pericentral (*CYP2E1, FETUB, HMGCS1*) and periportal (*APOC2, Saa1/Saa2, HAMP*) markers, which scRNA-seq alone was unable to distinguish. As an indication of the applicability of the WHV model to examine immune targets in HBV, our study found that most immune cells in woodchuck liver and PBMCs resembled human counterparts, including T-cell, monocyte and macrophage subsets, supporting translatable immune targets. Notably, tumour-associated exhausted T cells represent a promising therapeutic target given their important role in promoting viral tolerance and immune escape in many cancers.[14]

A well-described challenge related to transcriptionally profiling total liver homogenates is the fragility of hepatocytes, which leads to high cell death and consequent release of ambient RNA, which can contaminate cell preparations and complicate annotation. Filtering the liver homogenate datasets with DropletQC greatly improved the clarity of signals from the liver tissue data and removed clusters previously thought to be periportal hepatocytes and Kupffer cells.

However, the WHV-infected woodchuck model of HBV is not without its caveats. cHBV infection in humans is frequently associated with progressive liver fibrosis or cirrhosis which is infrequent in woodchucks with cWHV.[12] Moreover, progression to cWHV-induced HCC is more consistent and rapid,[12] whereas only 10-25% of chronically HBV-infected individuals develop HCC.[35] Finally, WHV frequently integrates around the *N-myc2* locus,[36] whereas HBV insertional mutagenesis is largely thought to be random.[37] Thus, findings related to WHV-triggered HCC development in woodchucks may not fully replicate processes expected to occur in HBV-induced liver cancer.

Taken together, our work characterising the immune cells in cWHV allows for hypothesis generation of potential immunotherapies that can be tested and analysed in the cWHV infection model for HBV-induced HCC. Future work may incorporate additional disease stages, multi-omic data, and validation of predicted cellular phenotypes. Taken together, these maps will enhance the utility of the woodchuck-WHV model and serve as a reference for the HBV community to examine the hepatic cellular microenvironment and intrahepatic immune responses, enabling the testing of antiviral and immunotherapies throughout WHV-induced inflammatory liver disease and HCC development.

Affiliations

[1]*Department of Molecular Genetics, University of Toronto, Toronto, Ontario, Canada;* [2]*The Donnelly Centre, University of Toronto, Toronto, Ontario, Canada;* [3]*Department of Immunology, University of Toronto, Toronto, Ontario Canada;* [4]*Ajmera Transplant Centre, Toronto General Hospital Research Institute, Toronto, Ontario, Canada;* [5]*The Centre for Applied Genomics, The Hospital for Sick Children, Toronto, Ontario, Canada;* [6]*Department of Laboratory Medicine and Pathobiology, University of Toronto, Toronto, Ontario, Canada;* [7]*Molecular Virology and Hepatology Research Group, Faculty of Medicine, Health Science Center, Memorial University of Newfoundland, St. John's, Newfoundland, Canada;* [8]*Department of Computer Science, University of Toronto, Toronto, Ontario, Canada*

Abbreviations

cHBV, chronic hepatitis B virus; (c)WHV, (chronic) woodchuck hepatitis virus; HCC, hepatocellular carcinoma; PBMC, peripheral blood mononuclear cell; PCLS, precision cut liver slice; PMA, phorbol 12-myristate 13-acetate; scRNA-seq, single-cell RNA sequencing; snRNA-seq, single-nucleus RNA sequencing.

Financial support

We acknowledge the University of Toronto McLaughlin Centre Accelerator Grants in Genomic Medicine awarded to I.D.M., G.D.B., S.A.M. the Canadian Liver Foundation's Team Grant in Hepatocellular Carcinoma to I.D.M., T.I.M., W.C.W.C., S.A.M., the UHN Foundation, and the Natural Sciences and Engineering Research Council (NSERC) Discovery Grant program RGPIN-2018-05958 to S.A.M. and the Canadian Institutes of Health Research (grant PJT 469829) to G.D.B.. J.A. has received a graduate student fellowship from the Canadian Network on Hepatitis C (CanHepC). CanHepC is funded by a joint initiative of the Canadian Institutes of Health Research (CIHR) (NHC-142832) and the Public Health Agency of Canada (PHAC). The Woodchuck reference genome was generated based on sequencing funded through the CanSeq150 program of CGEn, Canada's national platform for genome sequencing and analysis.

Conflict of interest

The authors declare no conflicts of interest pertaining to this manuscript.

Please refer to the accompanying ICMJE disclosure forms for further details.

Authors' contributions

S.A.M., G.D.B., and I.D.M. designed the study. S.L. and T.L. sequenced the genome. Z.A.C. annotated the genome. L.Y.L., D.C., S.C., X.-Z.M., L.W. and J.M. conducted liver experiments. Z.A.C. and J.A. performed the computational analysis. Z.A.C., X.W., T.I.M., and J.A. interpreted the data. C. T. performed the pathological review on the IHC. All authors contributed to the writing of the paper.

Data availability

The woodchuck genome sequence and annotation are available at https://doi.org/10.5281/zenodo.10855128. The raw RNA-seq data and data matrices output by Cell Ranger are available at the Gene Expression Omnibus (GEO) at accession numbers GSE264104 (scRNA-seq), GSE264107 (spatial), and GSE264112 (snRNA-seq). The single-cell and single-nucleus datasets are hosted by UCSC Cell Pre-publication browser (https://cells-test.gi.ucsc.edu/?ds=woodchuck-liver), final post publication browser at https://woodchuck-liver.cells.ucsc.edu. The code used to process the data can be found at https://github.com/14zac2/HealthyWoodchuckMap.

Acknowledgements

The authors acknowledge the Princess Margaret Genomics Centre, the Pathology Research Program and the Advanced Optical Microscopy Facility at University Health Network for their support and services. The authors acknowledge the Animal Resource Centre at the UHN for their support and services. The graphical abstract and select figures were created with Biorender.com.

Supplementary data

Supplementary data to this article can be found online at https://doi.org/10.1016/j.jhep.2025.12.030.

References

Author names in bold designate shared co-first authorship

[1] **MacParland SA**, **Liu JC**, **Ma X-Z**, et al. Single cell RNA sequencing of human liver reveals distinct intrahepatic macrophage populations. Nat Commun 2018;9:4383. https://doi.org/10.1038/s41467-018-06318-7.
[2] Aizarani N, Saviano A, Sagar, et al. A human liver cell atlas reveals heterogeneity and epithelial progenitors. Nature 2019;572:199–204. https://doi.org/10.1038/s41586-019-1373-2.
[3] Halpern KB, Shenhav R, Matcovitch-Natan O, et al. Single-cell spatial reconstruction reveals global division of labour in the mammalian liver. Nature 2017;542:352–356. https://doi.org/10.1038/nature21065.
[4] Michalopoulos GK. Liver regeneration after partial hepatectomy: critical analysis of mechanistic dilemmas. Am J Pathol 2010;176:2–13. https://doi.org/10.2353/ajpath.2010.090675.
[5] Global HIV, Hepatitis and STIs Programmes (HHS). Health Product Policy and Standards (HPS) WHO. Global hepatitis report 2024: action for access in low- and middle-income countries. World Health Organization; 2024.
[6] Guo W-N, Zhu B, Ai L, et al. Animal models for the study of hepatitis B virus infection. Zool Res 2018;39:25–31. https://doi.org/10.24272/j.issn.2095-8137.2018.013.
[7] Cornberg M, Lok AS, Terrault NA, et al. 2019 EASL-AASLD HBV Treatment Endpoints Conference Faculty. Guidance for design and endpoints of clinical trials in chronic hepatitis B - report from the 2019 EASL-AASLD HBV Treatment Endpoints Conference. Hepatology 2019. https://doi.org/10.1002/hep.31030.
[8] Menne S, Cote PJ. The woodchuck as an animal model for pathogenesis and therapy of chronic hepatitis B virus infection. World J Gastroenterol 2007;13:104–124.
[9] Michalak TI. Naturally occurring immunopathogenic model of HBV Infection, hepatitis B and HBV-associated hepatocellular carcinoma in the North American woodchuck, *Marmota monax*. J Immunol 2025;214:2504–2514. https://doi.org/10.1093/jimmun/vkaf231.
[10] Suresh M, Menne S. Recent drug development in the woodchuck model of chronic hepatitis B. Viruses 2022;14. https://doi.org/10.3390/v14081711.
[11] Mauda-Havakuk M, Mikhail AS, Starost MF, et al. Imaging, pathology, and immune correlates in the woodchuck hepatic tumor model. J Hepatocell Carcinoma 2021;8:71–83. https://doi.org/10.2147/JHC.S287800.
[12] Michalak TI. Diverse virus and host-dependent mechanisms influence the systemic and intrahepatic immune responses in the woodchuck model of hepatitis B. Front Immunol 2020;11:853. https://doi.org/10.3389/fimmu.2020.00853.
[13] Zhang C, Li J, Cheng Y, et al. Single-cell RNA sequencing reveals intrahepatic and peripheral immune characteristics related to disease phases in HBV-infected patients. Gut 2023;72:153–167. https://doi.org/10.1136/gutjnl-2021-325915.
[14] Liu LY, Ma X-Z, Ouyang B, et al. Nanoparticle uptake in a spontaneous and immunocompetent woodchuck liver cancer model. ACS Nano 2020;14:4698–4715. https://doi.org/10.1021/acsnano.0c00468.
[15] Hao Y, Hao S, Andersen-Nissen E, et al. Integrated analysis of multimodal single-cell data. BioRxiv 2020. https://doi.org/10.1101/2020.10.12.335331.
[16] Muskovic W, Powell JE. DropletQC: improved identification of empty droplets and damaged cells in single-cell RNA-seq data. Genome Biol 2021;22:329. https://doi.org/10.1186/s13059-021-02547-0.
[17] **Andrews TS**, **Atif J**, **Liu JC**, et al. Single-cell, single-nucleus, and spatial RNA sequencing of the human liver identifies cholangiocyte and mesenchymal heterogeneity. Hepatol Commun 2022;6:821–840. https://doi.org/10.1002/hep4.1854.
[18] 10x Genomics. PBMCs from a healthy donor: whole transcriptome analysis, single cell gene expression dataset by cell ranger 4.0.0. 2020. https://support.10xgenomics.com/single-cell-gene-expression/datasets/4.0.0/Parent_NGSC3_DI_PBMC. [Accessed 20 May 2024].
[19] Tietscher S, Wagner J, Anzeneder T, et al. A comprehensive single-cell map of T cell exhaustion-associated immune environments in human breast cancer. Nat Commun 2023;14:98. https://doi.org/10.1038/s41467-022-35238-w.
[20] Kumar BV, Ma W, Miron M, et al. Human tissue-resident memory T cells are defined by core transcriptional and functional signatures in lymphoid and mucosal sites. Cell Rep 2017;20:2921–2934. https://doi.org/10.1016/j.celrep.2017.08.078.
[21] Weinreich MA, Takada K, Skon C, Reiner SL, Jameson SC, Hogquist KA. KLF2 transcription-factor deficiency in T cells results in unrestrained cytokine production and upregulation of bystander chemokine receptors. Immunity 2009;31:122–130. https://doi.org/10.1016/j.immuni.2009.05.011.
[22] Wang Z, Wang Y, Yan Q, et al. FPR1 signaling aberrantly regulates S100A8/A9 production by CD14+FCN1hi macrophages and aggravates pulmonary pathology in severe COVID-19. Commun Biol 2024;7:1321. https://doi.org/10.1038/s42003-024-07025-4.
[23] Helft J, Anjos-Afonso F, van der Veen AG, Chakravarty P, Bonnet D, Reis e Sousa C. Dendritic cell lineage potential in human early hematopoietic progenitors. Cell Rep 2017;20:529–537. https://doi.org/10.1016/j.celrep.2017.06.075.
[24] Andrews TS, Nakib D, Perciani CT, et al. Single-cell, single-nucleus, and spatial transcriptomics characterization of the immunological landscape in the healthy and PSC human liver. J Hepatol 2024;80:730–743. https://doi.org/10.1016/j.jhep.2023.12.023.
[25] Lee JH, Lee BH, Jeong S, et al. Single-cell RNA sequencing identifies distinct transcriptomic signatures between PMA/ionomycin- and αCD3/αCD28-activated primary human T cells. Genomics Inform 2023;21:e18. https://doi.org/10.5808/gi.23009.
[26] Tang TJ, Kwekkeboom J, Laman JD, et al. The role of intrahepatic immune effector cells in inflammatory liver injury and viral control during chronic hepatitis B infection. J Viral Hepat 2003;10:159–167. https://doi.org/10.1046/j.1365-2893.2003.00412.x.
[27] Dudek M, Pfister D, Donakonda S, et al. Auto-aggressive CXCR6+ CD8 T cells cause liver immune pathology in NASH. Nature 2021;592:444–449. https://doi.org/10.1038/s41586-021-03233-8.
[28] Nkongolo S, Mahamed D, Kuipery A, et al. Longitudinal liver sampling in patients with chronic hepatitis B starting antiviral therapy reveals hepatotoxic CD8+ T cells. J Clin Invest 2023;133. https://doi.org/10.1172/JCI158903.
[29] Suresh M, Czerwinski S, Murreddu MG, et al. Innate and adaptive immunity associated with resolution of acute woodchuck hepatitis virus infection in adult woodchucks. Plos Pathog 2019;15:e1008248. https://doi.org/10.1371/journal.ppat.1008248.
[30] Corkum CP, Wiede LL, Ruble CL-A, et al. Identification of antibodies cross-reactive with woodchuck immune cells and activation of virus-specific and global cytotoxic T cell responses by anti-PD-1 and anti-PD-L1 in experimental chronic hepatitis B and persistent occult hepadnaviral infection. Front Microbiol 2022;13:1011070. https://doi.org/10.3389/fmicb.2022.1011070.
[31] Yan Q, Li M, Liu Q, et al. Molecular characterization of woodchuck IFI16 and AIM2 and their expression in woodchucks infected with woodchuck hepatitis virus (WHV). Sci Rep 2016;6:28776. https://doi.org/10.1038/srep28776.
[32] Fletcher SP, Chin DJ, Ji Y, et al. Transcriptomic analysis of the woodchuck model of chronic hepatitis B. Hepatology 2012;56:820–830. https://doi.org/10.1002/hep.25730.
[33] He Q-F, Xu Y, Li J, Huang Z-M, et al. CD8+ T-cell exhaustion in cancer: mechanisms and new area for cancer immunotherapy. Brief Funct Genomics 2019;18:99–106. https://doi.org/10.1093/bfgp/ely006.
[34] Williams JB, Hüppner A, Mulrooney-Cousins PM, et al. Differential expression of woodchuck toll-like receptors 1-10 in distinct forms of infection and stages of hepatitis in experimental hepatitis B virus infection. Front Microbiol 2018;9:3007. https://doi.org/10.3389/fmicb.2018.03007.
[35] Ozakyol A. Global epidemiology of hepatocellular carcinoma (HCC epidemiology). J Gastrointest Cancer 2017;48:238–240. https://doi.org/10.1007/s12029-017-9959-0.

[36] Chauhan R, Churchill ND, Mulrooney-Cousins PM, et al. Initial sites of hepadnavirus integration into host genome in human hepatocytes and in the woodchuck model of hepatitis B-associated hepatocellular carcinoma. Oncogenesis 2017;6:e317. https://doi.org/10.1038/oncsis.2017.22.

[37] Budzinska MA, Shackel NA, Urban S, et al. Cellular genomic sites of hepatitis B virus DNA integration. Genes 2018:9. https://doi.org/10.3390/genes9070365.

Keywords: Liver; Single Cell RNA sequencing; Spatial Transcriptomics; Single Nucleus RNA sequencing; Woodchuck; Marmota monax.
Received 9 January 2025; received in revised form 27 December 2025; accepted 29 December 2025; available online 22 January 2026